Role of weak interlayer coupling in ultrafast exciton-exciton annihilation in two-dimensional rhenium dichalcogenides

Sangwan Sim, 1,2,* Doeon Lee, 3,* Jekwan Lee, 4 Myungjun Cha, 4 Soonyoung Cha, 2 Wonhyeok Heo, 4,5 Sungjun Cho, 6 Wooyoung Shim, 6 Kyusang Lee, 3,7 Jinkyoung Yoo, 8 Rohit P. Prasankumar, 8 Hyunyong Choi ,4,† and Moon-Ho Jo ,2,9,‡ 1 Division of Electrical Engineering, Hanyang University, Ansan 15588, Korea 2 Center for Artificial Low Dimensional Electronic Systems, Institute for Basic Science (IBS), Pohang 37673, Korea 3 Department of Electrical and Computer Engineering, University of Virginia, Charlottesville, Virginia 22903, USA 4 Department of Physics and Astronomy, Institute of Applied Physics, Seoul National University, Seoul, 08826, Korea 5 School of Electrical and Electronic Engineering, Yonsei University, Seoul 03722, Korea 6 Department of Materials Science and Engineering, University of Virginia, Charlottesville, Virginia, 22903, USA 8 Center for Integrated Nanotechnologies, Los Alamos National Laboratory, Los Alamos, New Mexico 87545, USA 9 Department of Materials Science and Engineering, Pohang University of Science and Technology (POSTECH), Pohang 37673, Korea

(Received 7 February 2020; revised manuscript received 13 April 2020; accepted 21 April 2020; published 19 May 2020)

Strong interactions between excitons are a characteristic feature of two-dimensional (2D) semiconductors, determining important excitonic properties, such as exciton lifetime, coherence, and photon-emission efficiency. Rhenium disulfide (ReS_2), a member of the 2D transition-metal dichalcogenide (TMD) family, has recently attracted great attention due to its unique excitons that exhibit excellent polarization selectivity and coherence features. However, an in-depth understanding of exciton-exciton interactions in ReS_2 is still lacking. Here we used ultrafast pump-probe spectroscopy to study exciton-exciton interactions in monolayer (1L), bilayer (2L), and triple layer ReS_2 . We directly measure the rate of exciton-exciton annihilation, a representative Augertype interaction between excitons. It decreases with increasing layer number, as observed in other 2D TMDs. However, while other TMDs exhibit a sharp weakening of exciton-exciton annihilation between 1L and 2L, such behavior was not observed in ReS_2 . We attribute this distinct feature in ReS_2 to the relatively weak interlayer coupling, which prohibits a substantial change in the electronic structure when the thickness varies. This work not only highlights the unique excitonic properties of ReS_2 but also provides novel insight into the thickness dependence of exciton-exciton interactions in 2D systems.

DOI: 10.1103/PhysRevB.101.174309

I. INTRODUCTION

Over the past few years, two-dimensional transition metal dichalcogenides (TMDs), most often represented by MX_2 (M = Mo and W; X = S and Se), have gathered great attention due to their excellent excitonic properties, such as strong coupling with light [1,2], valley selectivity [3], and high electrical tunability [4,5]. In particular, strong quantum confinement and reduced dielectric screening lead to large exciton binding energies up to hundreds of meV [6,7], enabling stable excitons at room temperature. On the other hand, the large quantum confinement also causes strong scattering between excitons. This is usually observed as exciton-exciton annihilation (EEA), an Auger-type process in which a collision between two excitons leads to the recombination of one exciton, with the other excited to higher states [8–15]. Since EEA depopulates excitons rapidly and nonradiatively, it plays

a key role in determining exciton lifetimes and photoluminescence yield in 2D TMDs [13,16,17].

Rhenium dichalcogenides (ReX_2) are relatively new members of the 2D TMD family [Fig. 1(a)]. Compared to 2D MX_2 , Re X_2 have reduced in-plane crystal symmetry, accompanied by zigzag chains of rhenium atoms [red line in the bottom schematic in Fig. 1(a)] and a distorted 1T structure [18–20]. This anisotropic crystal structure gives rise to strongly anisotropic excitons with respect to linearly polarized light [21-23]. Recently, we have found that excitons in 2D ReS₂ show a light-polarization selective optical Stark effect [24,25] and coherent quantum beats [26], originating from their unique polarization dependence and large exciton binding energies. These studies have demonstrated that excitons in 2D rhenium dichalcogenides are promising candidates for realizing transparent and atomically thin ultrafast optical switches and modulators [24-26]. Very recently, EEA-like ultrafast dynamics has been observed in few-layer ReS₂ [27,28]. This result implies that EEA might affect the exciton lifetime and coherence time in ReX_2 , ultimately affecting the performance of ultrafast devices based on this nanomaterial.

^{*}These authors contributed equally to this work.

[†]Corresponding author: hy.choi@snu.ac.kr

[‡]Corresponding author: mhjo@postech.ac.kr

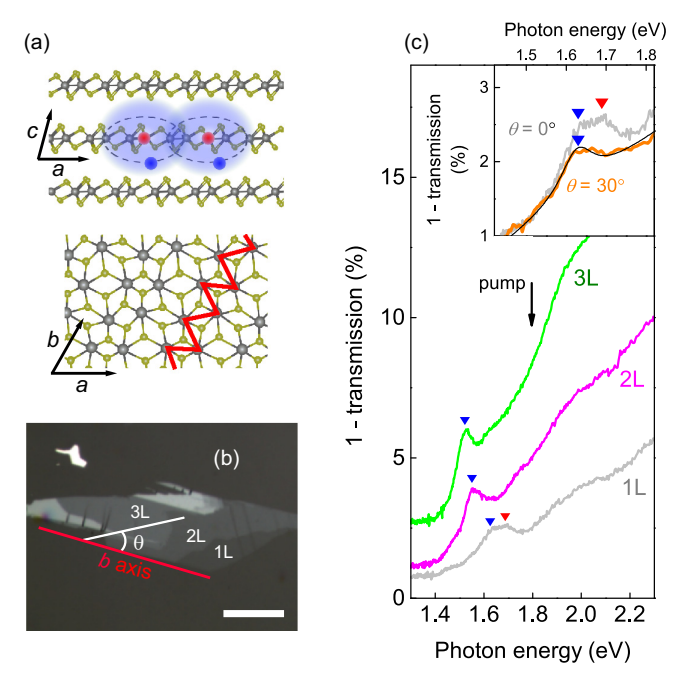


FIG. 1. (a) The upper and lower crystal structures represent side and top views of layered ReS₂, respectively. Gray (yellow) dots represent Re (S) atoms. Interactions between excitons are illustrated in the upper schematic. (b) Optical image of the 2D ReS₂ sample. θ defines the angle of the light polarization with respect to the crystal b axis (white line). Scale bar, 20 μ m. (c) Layer number-resolved 1-Tr spectra at $\theta = 0^{\circ}$. Blue (red) triangles indicate the resonance energies for E_1 (E_2). The black arrow indicates the pump photon energy. Inset: 1-Tr spectra of 1L at $\theta = 0^{\circ}$ (gray) and $\theta = 30^{\circ}$ (orange). The E_1 resonance is represented by a Lorentzian curve along with a linear background (black solid line).

EEA is also relevant to a fundamental issue in ReX_2 physics. In typical 2D TMDs, such as MX_2 , the electronic structure and the direct/indirect band-gap nature change with the number of layers due to interlayer coupling [1,2]. Accordingly, the rate of EEA also varies with layer number, because the electron-hole recombination process is largely dependent on the electronic band structure [10]. On the contrary, the interlayer coupling in ReX_2 has been believed to be extremely weak, because the formation of in-plane Re chains removes the energy benefits from the ordered stacking of adjacent layers. This has been supported by measurements of the thickness-independent vibrational responses [18,29] and poor thermal conduction between layers [30]. Also, theoretical calculations showed that, due to the weak interlayer coupling, the direct gap nature of ReS₂ persists for all layer thicknesses [18,31-33]. However, other theoretical studies found that ReX_2 exhibits a direct-indirect band-gap crossover as the layer number changes [34], as in other TMDs, and optical experiments observed meaningful thickness dependencies of the excitonic and vibrational properties [22,35,36]. These findings raise the question of how the interlayer coupling and the resulting electronic structure affect exciton-exciton interactions in ReX_2 , and suggest that the thickness dependence of EEA in Re X_2 will be different from those in typical 2D TMDs.

In this work we used time-resolved pump-probe spectroscopy to study ultrafast exciton dynamics and its thickness dependence in monolayer (1L), bilayer (2L), and triple layer (3L) ReS₂. For all layer thicknesses, we observe EEA dynamics that becomes more pronounced with increasing excitation intensity. The rate of EEA decreases with increasing layer number because the exciton binding energy gradually weakens with increasing sample thickness. However, unlike other TMDs (e.g., WS₂) that show a sharp drop in the EEA rate from one to two layers [10,11], such a strong thickness dependence was not observed in ReS2. This result suggests that the strength of the exciton-exciton interaction in ReS₂ is only weakly dependent on the layer number, due to the weak coupling between layers. This work not only provides novel insight into the thickness dependence of exciton-exciton interactions in 2D systems, but also provides intrinsic excitonic parameters, including EEA rates and exciton diffusion coefficients, that can be utilized in designing 2D-rheniumdichalcogenides-based ultrafast optoelectronic devices.

II. EXPERIMENT

ReS₂ flakes on a double-sided polished sapphire substrate were prepared by mechanical exfoliation of a bulk crystal [Fig. 1(b)]. The layer number was confirmed by optical transmission (Tr) spectroscopy (see below) and atomic force microscopy [37]. The steady-state Tr spectra [Fig. 1(c)] were obtained with radiation from a broadband continuous-wave laser source, in conjunction with a monochromator and a 50× objective lens. The percent transmission is defined by $(T_{\text{ReS2+Sub}}/T_{\text{Sub}}) \times 100$, where $T_{\text{ReS2+Sub}}$ (T_{Sub}) represent the intensity of the light beam transmitted through the ReS2 flake on the substrate (the bare substrate). Ultrafast pump-probe spectroscopy was performed using a 250 kHz Ti:sapphire regenerative amplifier system, where the frequency doubled output of an optical parametric amplifier and a white-light continuum generated in a sapphire disk served as the pump and probe beams, respectively. The \sim 110 fs duration laser pulses were linearly polarized; the polarization orientation angle (θ) is defined with respect to the crystal b axis [yellow line in Fig. 1(b)] [19,22]. A 50× objective lens focused the pump (probe) beam to a 2 (1) μ m spot on the sample. To investigate exciton dynamics, we measured the differential transmission (DT), which is defined by $\Delta T/T_0 = (T_p T_0$)/ T_0 . Here, $T_p(T_0)$ represents the intensity of the probe beam transmitted through the sample with (without) the pump. The photon energy (E_{ph}) and the polarization of the pump were fixed at 1.8 eV [arrow in Fig. 1(c)] and $\theta = 0^{\circ}$, respectively. All measurements were performed at room temperature under ambient conditions.

III. RESULTS AND DISCUSSION

We first identify the resonance energies of the lowest exciton (E_1) in the 1L, 2L, and 3L regions using Tr spectroscopy. The main panel of Fig. 1(c) displays the measured 1-Tr spectra at $\theta=0^\circ$; E_1 peaks are well resolved in 2L (magenta) and 3L (green), as indicated by the blue triangles at 1.55 and 1.52 eV, respectively. Note that, although the second lowest exciton (E_2) is located close to E_1 , it is significantly suppressed at $\theta=0^\circ$ in 2L and 3L due to its strong anisotropy, such that E_1 dominates the 1-Tr response [22,24,26]. In the following

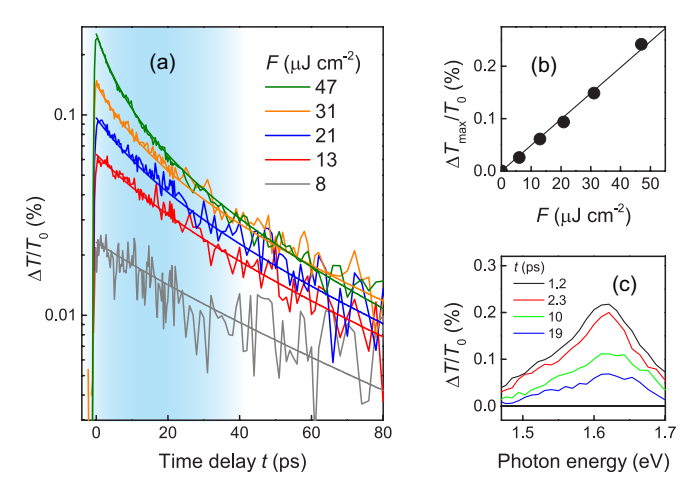


FIG. 2. (a) DT traces probed at $\theta = 30^{\circ}$ and a photon energy of 1.62 eV in 1L ReS₂ with varying F are shown with their fit lines (see main text). The blue shading indicates the region in which the fast decay component grows with increasing F due to EEA. (b) Corresponding maximum DT signal as a function of F. The solid line is a linear guide to the eye. (c) DT spectra for several t at $F = 47 \,\mu\mathrm{J}\,\mathrm{cm}^{-2}$.

ultrafast DT measurements, the probe polarization angle is fixed at $\theta = 0^{\circ}$ to measure the response of E_1 for 2L and 3L. On the contrary, the exciton response in 1L at $\theta = 0^{\circ}$ shows two distinct exciton peaks, E_1 (blue triangle) and E_2 (red triangle), as shown by the gray line in Fig. 1(c). This is because the orientation angle of E_2 in 1L is closer to $\theta = 0^{\circ}$ than in thicker layers, where it is closer to 90 deg [22]. To minimize the contribution of E_2 , the probe polarization in DT spectroscopy of 1L is set to $\theta = 30^{\circ}$, for which E_2 is suppressed and E_1 dominates the optical response, as shown by the orange line in the inset of Fig. 1(c). There the 1-Tr spectrum at $\theta = 30^{\circ}$ (i.e., the orange line) is well fit by a single Lorentzian curve for E_1 centered at 1.62 eV (black smooth line). All of the identified exciton energies are in good agreement with literature values [22]. In the following ultrafast DT measurements, the probe photon energies are set at the E_1 peaks for each layer number (i.e., 1.62, 1.55, and 1.52 eV for 1L, 2L, and 3L, respectively) to investigate the dynamics of the lowest energy excitons.

Let us now explore the thickness-dependent exciton dynamics. We begin with a time-resolved study of 1L. Figure 2(a) shows the measured DT traces as a function of pumpprobe time delay (t). We assume that these traces reflect the dynamics of pump-generated excitons, due to the following reasons. First, the initially photoinjected electron-hole pairs can form stable excitons, since the exciton binding energy of 1L ReS₂ (~0.7-1 eV) far exceeds the thermal energy at room temperature [31,32,38]. Second, the pump-generated electron-hole pair density per layer $n_0 \sim FA/E_{\rm ph}m$ ranges from 2.3 \times 10¹¹ to 1.3 \times 10¹² cm⁻², which is lower than the Mott threshold of typical 2D TMDs ($\sim 10^{13}$ cm⁻²) [39–41] (here, F is the pump fluence ranging from 8 to $47 \,\mu\mathrm{J}\,\mathrm{cm}^{-2}$, the absorbance $(A \sim -\log Tr)$ [42] is taken from Fig. 1(c), and m is the layer number). This is corroborated by the linear F dependence of the DT peaks [Fig. 2(b)], which indicates that n_0 is below the saturation limit [8]. Third, the DT spectra exhibit shapes similar to a single Lorentzian peak at the E_1 resonance regardless of t, as shown in Fig. 2(c), indicating that DT signals arise from resonance bleaching due to phase-space filling by pump-generated excitons. Unbound photoexcited carriers can also cause exciton bleaching via the screening of the Coulomb interaction [43]. However, it is unlikely in our case because these carriers usually lead to a significant increase in the scattering rate and consequent linewidth broadening that is not observed in our DT spectra [Fig. 2(c)] [44].

With this understanding we now discuss the F-dependent exciton dynamics for 1L. In Fig. 2(a) we can see that, while the DT traces exhibit a single-exponential-like decay at low F ($<21 \,\mu\mathrm{J\,cm^{-2}}$), an additional fast decay component emerges and becomes more pronounced with increasing F at $t < 30 \,\mathrm{ps}$, as indicated by the blue shaded region. Such F-dependent behavior of the fast component is the hallmark of EEA, because this Auger-type interaction is more strongly activated in the high density regime [8,9]. To confirm this, we consider a typical rate equation model describing the dynamics of the exciton density (N), given by

$$dN/dt = -N^2/\tau_1 - N/\tau_2,$$
 (1)

where τ_1 and τ_2 are exciton lifetimes [10,14,45]. The first term on the right-hand side in Eq. (1) describes bimolecular recombination, which can be used to account for the nonradiative recombination of two excitons in the EEA process [10,45]. We thus define the rate of EEA by $\gamma = 1/\tau_1$. τ_2 corresponds to the exciton lifetime without EEA, which will be discussed in detail below. Assuming the transient exciton density is proportional to the DT amplitude, the rate equation yields [10]

$$\frac{\Delta T}{T_0}(t) \propto N(t) = \frac{\exp(-t/\tau_2)}{1/n_0 + \gamma \tau_2 [1 - \exp(-t/\tau_2)]}.$$
 (2)

Figure 2(a) shows that Eq. (2) fits all sets of DT data well, where just varying n_0 with fixed $\gamma = 0.078 \pm 0.015$ cm² s⁻¹ and $\tau_2 \sim 60$ ps is enough to reproduce all the data. Note that, although these DT traces are probed at $\theta = 30^{\circ}$, the probe polarization does not have a significant effect on the dynamics of excitons (Fig. S2 of Ref. [37]) for all thicknesses. The lack of probe polarization dependence indicates that the E_2 exciton is not significantly contributing to the observed dynamics [38].

We next proceed by investigating exciton dynamics for thicker regions. Figures 3(a) and 3(b) display F-resolved DT traces for 2L and 3L, respectively (DT spectra and F-dependent maximum DT values are shown in Fig. S3 of Ref. [37]). Although the overall decay timescales are larger compared to 1L, the dynamics in both 2L and 3L become faster with increasing F [see shaded regions in Figs. 3(a) and 3(b)], which is a clear signature of EEA. The DT traces are also well fit by Eq. (2) with F-independent EEA rates ($\gamma = 0.047 \pm 0.016 \, \text{cm}^2 \, \text{s}^{-1}$ for 2L and $\gamma = 0.011 \pm 0.005 \, \text{cm}^2 \, \text{s}^{-1}$ for 3L), confirming the occurrence of EEA. τ_2 values for all fluences are almost unchanged for both 2L (~83 ps) and 3L (~139 ps) except for the lowest F in 3L [gray line in Fig. 3(b)], for which τ_2 shortens to ~110 ps. We found no signature of EEA in bulk ReS₂ [37].

Physically, pump photoexcitation at 1.8 eV directly excite excitons although the photon energy is somewhat higher than the exciton resonance energies [1.62 eV for 1L, 1.55 eV for

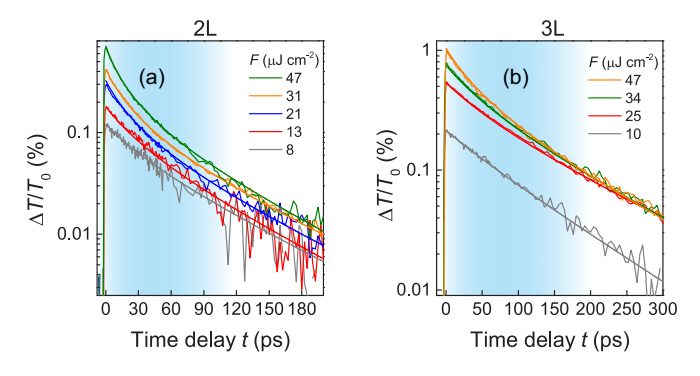


FIG. 3. *F*-dependent DT traces at $\theta = 0^{\circ}$ measured in (a) 2L and (b) 3L ReS₂, with corresponding fits. The blue shadings represent the regions where the fast exciton dynamics due to EEA are clearly seen.

2L, and 1.52 eV for 3L; Fig. 1(c)]. This is because 2D ReS₂ has large exciton binding energies up to hundreds of meV (e.g., \sim 0.7–1 eV for 1L and 0.4 eV for 2L [31,32]), such that the quasiparticle band gap energies are estimated to be larger than or comparable to the pumping energy. Subsequently, a fraction of the excitons will be annihilated through EEA (depending on their density) while the rest eventually recombine, likely through phonon-assisted recombination and/or traps. We will first discuss the slower, non-EEA dynamics represented by τ_2 , which is often associated with trap-mediated exciton depopulation by defects or impurities in 2D TMDs [9,11,46,47]. Since surface layers have much larger defect densities than other layers, trap-mediated decay will be a larger contribution for thinner samples [48], in agreement with the observed trend that τ_2 decreases with decreasing layer number (~60 ps for 1L, ~83 ps for 2L, and ~139 ps for 3L). In addition, this mechanism usually exhibits slower decay dynamics with increasing F, due to the decrease in unoccupied trap sites when the density of excitons is comparable with

that of traps [9,49,50]. This trap saturation effect may explain the observation that τ_2 at the lowest F is smaller than those measured at higher Fs in 3L. In contrast, we observe no Fdependence of τ_2 in 1L and 2L, indicating no saturation of trap sites. This is probably because the densities of initially unoccupied trap states in the thinner layers (1L and 2L) are likely larger than that of 3L, and the relatively strong EEA in 1L and 2L leads to fast depopulation of excitons [46,47]. Also, the absence of trap saturation features in 1L and 2L agrees with the fact that the maximum density of initially excited excitons ($\sim 1.4 \times 10^{12} \, \text{cm}^{-2}$) is lower than the trap density of 2D ReS₂ flakes known from literature ($\sim 10^{13}$ cm⁻²) [51]. We note that the observed τ_2 values for 3L are also consistent with the recently reported phonon-assisted electron-hole recombination time in 3L ReS₂ (~100 ps), indicating that this mechanism may also contribute to the observed τ_2 [27].

Next, we compare the obtained EEA rates with those in other TMDs. From now on, we will use subscripts to refer to the layer number of γ to avoid confusion (e.g., γ for 1L is γ_{1L}). As summarized in Fig. 4(a), γ_{1L} in 1L ReS₂ is comparable to some of the reported γ_{1L} values in other TMDs [8–15]. However, its thickness dependence exhibits quite different behavior. While γ in WS₂ is reduced by two orders of magnitude as the layer number changes from 1L to 2L [10], ReS₂ shows relatively weak thickness dependence. This feature is better displayed in Fig. 4(b), where the ratio γ_{1L}/γ_{2L} is indicated by red (\sim 2 for ReS₂) and green (\sim 50 for WS₂) dashed lines, respectively. On the contrary, γ in ReS₂ and WS₂ in Fig. 4(b) shows a similar layer dependence for 2L and 3L: γ_{2L}/γ_{3L} ratios in ReS₂ and WS₂ are \sim 5 (orange dashed line) and \sim 3 (blue dashed line), respectively.

To figure out this anomalous layer number dependence, we first consider the effect of exciton diffusion on EEA. In our measurements, the density of initially excited excitons ranges from $\sim 2.3 \times 10^{11}$ to $\sim 1.4 \times 10^{12}$ cm⁻², and the corresponding average separation of excitons is $\sim 9-21$ nm. This spacing

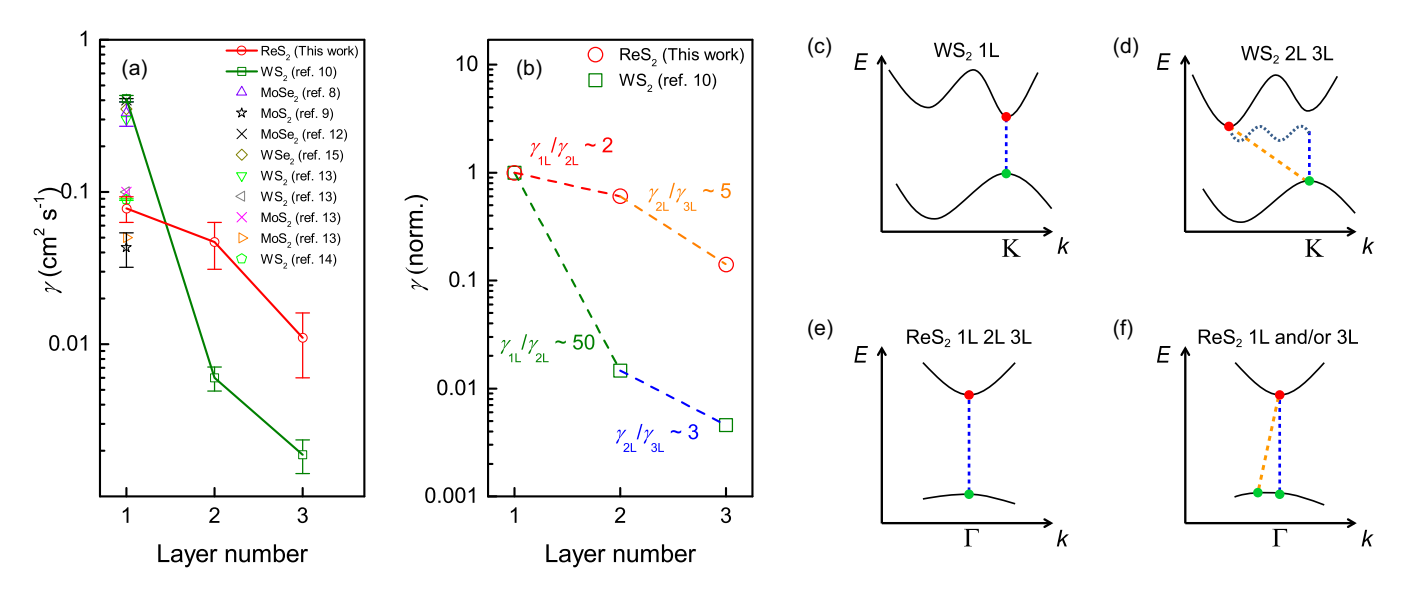


FIG. 4. (a) Comparison of EEA rates in ReS₂ obtained in this work (red circles) with those of other TMDs taken from the literature. (b) EEA rates normalized by the value for 1L in ReS₂ (red circles) and WS₂ (green squares; Ref. [10]). The ratios of EEA rates for adjacent layer numbers are also indicated. (c)–(h) Simplified band structures for (c) and (d) WS₂ and (e) and (f) ReS₂. Red (green) dots are excited electrons (holes). Blue and orange dashed lines represent the direct and indirect gaps, respectively.

TABLE I. Thickness-dependent EEA rates, exciton lifetimes without EEA, exciton diffusion coefficients and exciton diffusion lengths.

Layer number	EEA rate γ (cm ² s ⁻¹)	Exciton lifetime without EEA $ au_2$ (ps)	Exciton diffusion coefficient D (cm ² s ⁻¹)	Exciton diffusion length L (nm)
1	0.078 ± 0.015	59 ± 3	7 ± 1 16 ± 2 22 ± 1	~210
2	0.047 ± 0.016	83 ± 7		~360
3	0.011 ± 0.005	139 ± 10		~530

is larger than the exciton Bohr radii in typical 2D TMDs $(\sim 0.6-1.7 \text{ nm})$ [15,52–54], indicating that pump-generated excitons are sparsely distributed in our F range. In this case, the exciton diffusion coefficient (D) should be considered in understanding EEA, because the diffusion precedes the exciton-exciton interaction [10,13,15]. Moreover, it was recently reported that the hole effective mass in ReS₂ can significantly increase in the 1L limit [32,34]. Thus one might expect that the exciton diffusivity will be largely reduced for 1L, and consequently EEA will be much lower. It is thus important to measure D to accurately understand the influence of exciton diffusion on γ . Therefore, we performed pump-probe spatial mapping experiments to obtain D for 1-3L [38,46,55,56]. The resultant D and corresponding diffusion lengths $(L \sim \sqrt{D\tau_2})$ [38] are displayed with other obtained parameters in Table I (details of the experiments and data analysis are discussed in the Appendix). The measured D values are about two or three orders of magnitude larger than γ for all layer numbers, indicating that nearly all excitons diffuse far enough to interact with other excitons (and thus undergo EEA). This allows us to discuss the thickness dependence of the exciton-exciton interaction merely by comparing γ without including D (the Appendix provides a more detailed explanation) [10,37]. Our data thus demonstrates that diffusion of excitons does not play a significant role in EEA dynamics.

We next consider exciton binding energies. The larger the exciton binding energy, the stronger the Coulomb potential for exciton-exciton interactions [52] and the higher the Auger recombination rate [57]. Since most monolayer TMDs have large exciton binding energies up to several hundreds of meV, due to strong quantum confinement and reduced dielectric screening [7,31,32,53], exciton-exciton interactions in them are usually strong as well [52]. Stacking additional layers screens the electron-hole Coulomb interaction, weakening the exciton binding energy. This screening effect plays a key role in the decrease in exciton binding energy with increasing layer number in general 2D systems [7,31,58,59], which is in line with the decrease in γ with increasing layer number in both ReS₂ and WS₂ [Fig. 4(a) and Table I]. However, it does not explain the large difference in γ_{1L}/γ_{2L} values for ReS_2 and WS_2 [red and green dashed lines in Fig. 4(b)]. According to a recent theoretical study, although the direct electronic interlayer coupling in ReS₂ is relatively weak, the interlayer screening is significant, as in other TMDs, such that the exciton binding energy is reduced by about half as the layer number changes from 1L to 2L [32]. This reduction is almost the same as those in other TMDs, including WS₂ [7,60]. Thus, the exciton binding energy is unlikely to cause the large difference in γ_{1L}/γ_{2L} values for ReS₂ and WS₂ [Fig. 4(b)].

Finally, let us consider the effect of the electronic structure on EEA. The fundamental gap of 1L WS2 is direct, because both the CBM and the VBM are at the K point [Fig. 4(c)]. However, in 2L and thicker WS₂ [Fig. 4(d)], the position of the CBM is changed by interlayer coupling, such as interlayer overlap between electron clouds [7]. This causes the fundamental gap to become indirect, where exciton recombination via the EEA process requires the assistance of phonons (illustrated by the wavy line). Thus, EAA for larger layer thicknesses is less effective than that in 1L WS₂ [10]. 1L ReS₂ is also known to be a direct gap semiconductor, where the CBM and the VBM are at the Γ point [Fig. 4(e)]. However, in comparison with MX_2 , the electronic structure of ReS2 does not undergo significant changes with layer number, due to the relatively weak interlayer coupling in this system; therefore, the fundamental gap remains direct in thicker layers [Fig. 4(e)] [18,31-33]. This suggests that the lack (presence) of a sharp drop in γ for 1L-2L ReS₂ (WS₂) can be attributed to the relatively weak (strong) change in the electronic structure. For 2L-3L, a sharp drop in γ was not observed in both ReS₂ and WS₂ [Fig. 4(b)], agreeing with the fact that the electronic structure remains similar for 2L and thicker layers in both materials, even though they have different direct/indirect band-gap nature (i.e., direct for ReS2 and indirect for non-1L WS₂). This result further supports the idea that γ drops sharply only when the electronic structure strongly changes. Therefore, the relatively gentle drop in γ for 1-2L ReS₂ is due to the weak change in the electronic structure, which results from the weak interlayer coupling.

We note that other theoretical studies have reported different results on the direct/indirect band-gap nature of ReS₂ [27,34]. Despite these discrepancies, the common result is that the highest valence band near the Γ point is fairly flat for 1L and/or few layers, due to the strongly localized orbitals of Re atoms [Fig. 4(f)] [27,32,34]. The position of the VBM can be slightly displaced from the Γ point, depending on the calculation method, resulting in a change in the direct/indirect nature for a certain layer number. However, this subtle change in ReS₂, due to the relatively weak interlayer coupling, is still very different from the significant variations of the electronic structure seen in other TMDs [Figs. 4(c) and 4(d)]. Also, even when the fundamental gap in ReS₂ is calculated to be indirect, the energy difference between the indirect and direct gaps is much smaller than the thermal energy at room temperature $(\sim 26 \text{ meV})$, and thus is not expected to significantly affect our results.

IV. CONCLUSION

In summary, we have investigated exciton-exciton interactions in 2D ReS₂ and its thickness dependence using ultrafast pump-probe spectroscopy. We directly measured the rate of exciton annihilation, which decreases with increasing layer number, as in other TMDs. However, the sharp drop in the EEA rate between 1L and 2L, observed in other TMDs,

was not observed in ReS2. To understand this difference, we considered three factors that could affect the exciton-exciton interaction. First, we directly measured exciton diffusion coefficients, which are unlikely to play a key role in determining the thickness dependence of EEA because they are much higher than the rates of EEA for all layer numbers. Second, the exciton binding energy, which decreases with increasing thickness, is responsible for the monotonic decrease in EEA with layer number, but cannot explain the difference in the EEA rate ratios between ReS₂ and other TMDs for 1-2L. In fact, we can attribute the absence of a sharp drop in the EEA rate for ReS₂ to the relatively weak interlayer coupling, which prohibits a significant change in the electronic structure when the layer number changes (unlike conventional TMDs like WS₂). Our study thus not only provides unprecedented insight into the thickness dependence of exciton-exciton interactions in 2D systems, but also provides layer number-dependent parameters, such as EEA rates as well as exciton diffusion coefficients and lengths, that can be utilized in designing ReS₂-based optoelectronic devices.

ACKNOWLEDGMENTS

S.S. was supported by the NRF through the government of Korea (MSIP) (Grant NRF-2019R1F1A1063457) and the Korea Basic Science Institute under the R&D program (Project No. C030440) supervised by the Ministry of Science and ICT. J.L., M.C., W.H., and H.C. were supported by the NRF through the government of Korea (MSIP) (Grant No. 2018R1A2A1A05079060, the Creative Materials Discovery Program (Grant No. 2017M3D1A1040828), and the Institute for Basic Science (IBS) (Korea under Project Code IBS-R014-G1-2018-A1), and Scalable Quantum Computer Technology Platform Center (Grant 2019R1A5A1027055). D.L. and K.L. were supported from the U.S. National Science Foundation (NSF) under Grant CMMI-1825256. M.-H.J. and S.C. were supported by the Institute for Basic Science (IBS), Korea (project code IBS-R014-A1). This work was performed, in part, at the Center for Integrated Nanotechnologies, an Office of Science User Facility operated for the U.S. Department of Energy (DOE) Office of Science by Los Alamos National Laboratory and Sandia National Laboratories, and was also supported by the LANL LDRD program.

APPENDIX: MEASUREMENT OF EXCITON DIFFUSION

As discussed in the main text, exciton diffusion should be considered in analyzing EEA because initially excited excitons are sparsely distributed in our F range. Thus, we performed spatially resolved pump-probe mapping measurements to obtain layer number-dependent exciton diffusion coefficients. We measured DT profiles while scanning the position of the probe beam (x) with respect to the fixed pump center, as illustrated in Fig. 5(a). The scanning direction is chosen to be parallel to the crystal b axis. Figure 5(b) shows the measured DT profile for 1L as a function of t and x. We can see that the spatial width of the DT profile enlarges with t; corresponding data (dots) and Gaussian fits (solid lines) at two different time delays are shown in Fig. 5(c). This result

directly shows that excitons diffuse out of the initially excited region.

To obtain the diffusion coefficient, we consider a rate equation describing the diffusion-related exciton dynamics, given by [10]

$$\frac{\partial N(x,t)}{\partial t} = D\nabla^2 N(x,t) - \frac{N(x,t)}{\tau},\tag{A1}$$

where D is the exciton diffusion coefficient. Assuming a Gaussian spatial distribution of excitons, the solution of Eq. (A1) is

$$N(x,t) = \frac{\sigma_0^2 n_0}{\sigma^2(t)} \exp\left(-\frac{t}{\tau_{\rm E}}\right) \exp\left(-\frac{x^2}{\sigma^2(t)}\right),\tag{A2}$$

where

$$\sigma^2(t) = \sigma_0^2 + 4Dt \tag{A3}$$

is the Gaussian width of the spatial exciton distribution at t. This result indicates that we can obtain D by fitting Eq. (A3) to the measured squared Gaussian width of DT profiles [black open squares in Fig. 5(d)]. The acquired D at 1L is $7.4 \pm 1.4 \, \mathrm{cm^2 \, s^{-1}}$, roughly agreeing with a previous study [2]. In a similar way, we measure D at $2L (16 \pm 1.9 \, \mathrm{cm^2 \, s^{-1}})$ and $3L (21 \pm 1.4 \, \mathrm{cm^2 \, s^{-1}})$, as displayed in Fig. 5(d) (corresponding temporal evolutions of DT profiles are shown in Fig. 6). We also estimate the corresponding exciton diffusion length, which is defined by $L = \sqrt{D\tau}$. The resultant D and L values are summarized in Table I in the main text. There we can see that D increases with increasing layer number. This behavior

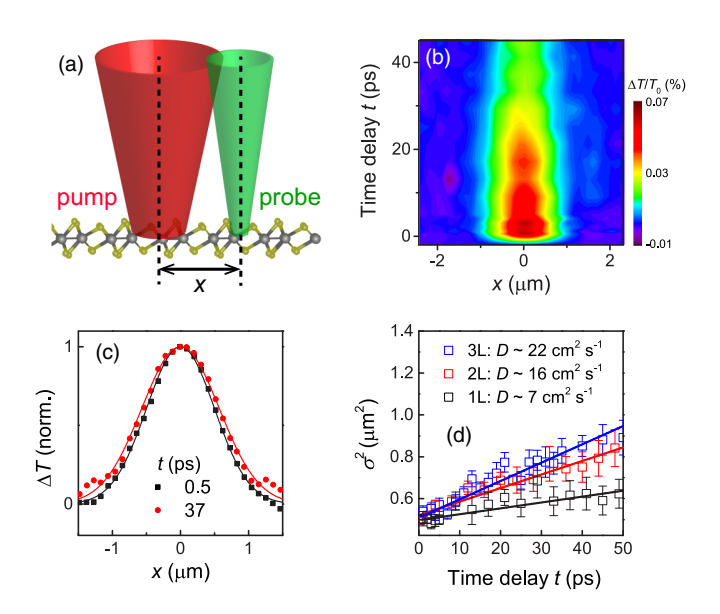


FIG. 5. (a) A schematic describing the spatiotemporal DT measurements. x represents the position of the probe beam with respect to the pump center. (b) DT signals at 1L as a function of t and x. The pump fluence is $F=13~\mu\mathrm{J}~\mathrm{cm}^{-2}$. (c) Spatial profiles of the DT in 1L at $t=0.5~\mathrm{ps}$ (black dots) and $t=37~\mathrm{ps}$ (red dots). The solid curves are corresponding Gaussian fits. (d) Squared Gaussian width of the spatial DT profiles as a function of t at 1L (black squares), 2L (red squares), and 3L (blue squares). The linear solid lines are fits (see the text).

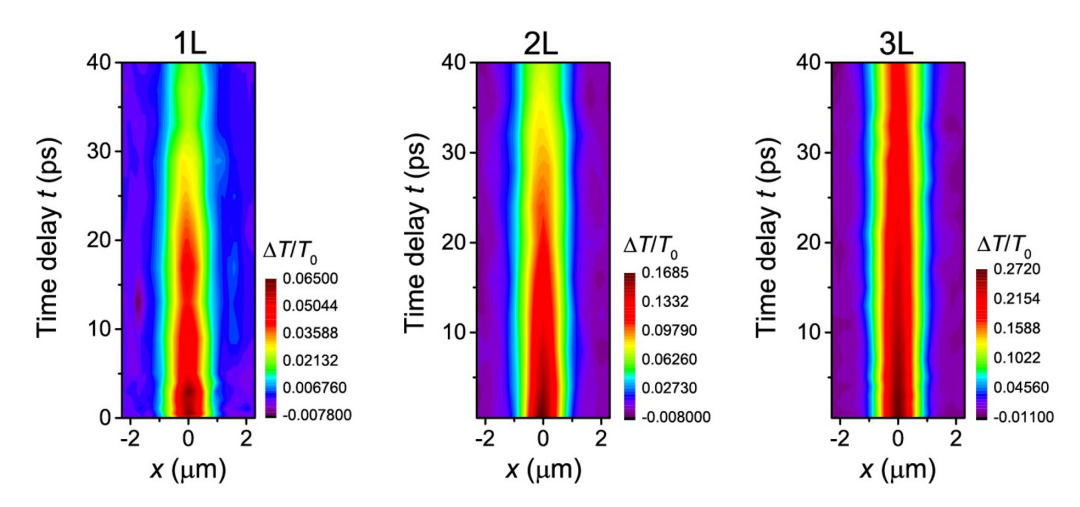


FIG. 6. DT signals as a function of x and t for 1L (left), 2L (middle), and 3L (right). Experimental conditions are described in the caption of Fig. 5.

may reflect the fact that the defect density decreases with increasing layer number.

Now let us discuss the relation between D and EEA. This diffusion-mediated EEA can be described by the reaction equation $E+E \leftrightarrow EE \rightarrow E$, whose overall interaction rate corresponds to γ [10,11]. Here two excitons (E + E) move toward each other with the rate of D to form an exciton pair (EE) in which the exciton spacing becomes small enough for EEA to occur. Then, the annihilation takes place (EE \rightarrow E) with the rate of k, which is the parameter that is closely associated with the annihilation cross section and the interaction probability. Thus k is of particular importance for understanding and comparing the strength of exciton-exciton

interaction. It is known that k can determined from γ and D through the relationship given by

$$k \sim \frac{\gamma}{1 - (\gamma/D)}.\tag{A4}$$

However, for all layer numbers, D is about two or three orders of magnitude larger than γ , such that k in Eq. (A4) can be approximated to be γ (i.e., $k \sim \gamma$). This means that D has little effect on the strength of the pure interexciton interaction, even though D varies with the layer number, as discussed by Yuan *et al.* [10]. This result guarantees that we can discuss the layer number dependence of the exciton-exciton interaction merely by comparing γ without considering D.

^[1] K. F. Mak, C. Lee, J. Hone, J. Shan, and T. F. Heinz, Phys. Rev. Lett. 105, 136805 (2010).

^[2] A. Splendiani, L. Sun, Y. Zhang, T. Li, J. Kim, C.-Y. Chim, G. Galli, and F. Wang, Nano Lett. 10, 1271 (2010).

^[3] X. Xu, W. Yao, D. Xiao, and T. F. Heinz, Nat. Phys. 10, 343 (2014).

^[4] K. F. Mak, K. He, C. Lee, G. H. Lee, J. Hone, T. F. Heinz, and J. Shan, Nat. Mater. 12, 207 (2012).

^[5] S. Wu, J. S. Ross, G. Bin Liu, G. Aivazian, A. Jones, Z. Fei, W. Zhu, D. Xiao, W. Yao, D. Cobden, and X. Xu, Nat. Phys. 9, 149 (2013).

^[6] A. Chernikov, T. C. Berkelbach, H. M. Hill, A. Rigosi, Y. Li, O. B. Aslan, D. R. Reichman, M. S. Hybertsen, and T. F. Heinz, Phys. Rev. Lett. 113, 076802 (2014).

^[7] H. P. Komsa and A. V. Krasheninnikov, Phys. Rev. B 86, 241201(R) (2012).

^[8] N. Kumar, Q. Cui, F. Ceballos, D. He, Y. Wang, and H. Zhao, Phys. Rev. B 89, 125427 (2014).

^[9] D. Sun, Y. Rao, G. a. Reider, G. Chen, Y. You, L. Brézin, A. R. Harutyunyan, and T. F. Heinz, Nono Lett. 14, 5625 (2014).

^[10] L. Yuan and L. Huang, Nanoscale 7, 7402 (2015).

^[11] L. Yuan, T. Wang, T. Zhu, M. Zhou, and L. Huang, J. Phys. Chem. Lett. 8, 3371 (2017).

^[12] B. Liu, Y. Meng, X. Ruan, F. Wang, W. Liu, F. Song, X. Wang, J. Wu, L. He, R. Zhang, and Y. Xu, Nanoscale 9, 18546 (2017).

^[13] Y. Yu, Y. Yu, C. Xu, A. Barrette, K. Gundogdu, and L. Cao, Phys. Rev. B 93, 201111(R) (2016).

^[14] P. D. Cunningham, K. M. McCreary, and B. T. Jonker, J. Phys. Chem. Lett. 7, 5242 (2016).

^[15] S. Mouri, Y. Miyauchi, M. Toh, W. Zhao, G. Eda, and K. Matsuda, Phys. Rev. B 90, 155449 (2014).

^[16] M. Amani, P. Taheri, R. Addou, G. H. Ahn, D. Kiriya, D. H. Lien, J. W. Ager, R. M. Wallace, and A. Javey, Nano Lett. 16, 2786 (2016).

^[17] O. Salehzadeh, N. H. Tran, X. Liu, I. Shih, and Z. Mi, Nano Lett. 14, 4125 (2014).

^[18] S. Tongay, H. Sahin, C. Ko, A. Luce, W. Fan, K. Liu, J. Zhou, Y. S. Huang, C. H. Ho, J. Yan, D. F. Ogletree, S. Aloni, J. Ji, S. Li, J. Li, F. M. Peeters, and J. Wu, Nat. Commun. 5, 3252 (2014).

^[19] D. A. Chenet, O. B. Aslan, P. Y. Huang, C. Fan, A. M. van der Zande, T. F. Heinz, and J. C. Hone, Nano Lett. 15, 5667 (2015).

^[20] M. Rahman, K. Davey, and S. Z. Qiao, Adv. Funct. Mater. 27, 1606129 (2017).

^[21] C. H. Ho, P. C. Liao, Y. S. Huang, and K. K. Tiong, Phys. Rev. B 55, 15608 (1997).

- [22] O. B. Aslan, D. A. Chenet, A. M. Van Der Zande, J. C. Hone, and T. F. Heinz, ACS Photon. 3, 96 (2016).
- [23] C. H. Ho and Z. Z. Liu, Nano Energy 56, 641 (2019).
- [24] S. Sim, D. Lee, M. Noh, S. Cha, C. H. Soh, J. H. Sung, M. H. Jo, and H. Choi, Nat. Commun. 7, 13569 (2016).
- [25] S. Sim, D. Lee, J. Lee, H. Bae, M. Noh, S. Cha, M.-H. Jo, K. Lee, and H. Choi, Nano Lett. 19, 7464 (2019).
- [26] S. Sim, D. Lee, A. V. Trifonov, T. Kim, S. Cha, J. H. Sung, S. Cho, W. Shim, M.-H. Jo, and H. Choi, Nat. Commun. 9, 351 (2018).
- [27] X. Wang, K. Shinokita, H. E. Lim, N. B. Mohamed, Y. Miyauchi, N. T. Cuong, S. Okada, and K. Matsuda, Adv. Funct. Mater. 29, 1806169 (2019).
- [28] K. P. Dhakal, H. Kim, S. Lee, Y. Kim, J. D. Lee, and J. H. Ahn, Light Sci. Appl. 7, 98 (2018).
- [29] F. Liu, S. Zheng, A. Chaturvedi, V. Zólyomi, J. Zhou, Q. Fu, C. Zhu, P. Yu, Q. Zeng, N. D. Drummond, H. J. Fan, C. Kloc, V. I. Fal'ko, X. He, and Z. Liu, Nanoscale 8, 5826 (2016).
- [30] H. Jang, C. R. Ryder, J. D. Wood, M. C. Hersam, and D. G. Cahill, Adv. Mater. 29, 1700650 (2017).
- [31] H.-X. Zhong, S. Gao, J.-J. Shi, and L. Yang, Phys. Rev. B 92, 115438 (2015).
- [32] J. P. Echeverry and I. C. Gerber, Phys. Rev. B 97, 075123 (2018).
- [33] E. Liu, Y. Fu, Y. Wang, Y. Feng, H. Liu, X. Wan, W. Zhou, B. Wang, L. Shao, C.-H. Ho, Y.-S. Huang, Z. Cao, L. Wang, A. Li, J. Zeng, F. Song, X. Wang, Y. Shi, H. Yuan, H. Y. Hwang, Y. Cui, F. Miao, and D. Xing, Nat. Commun. 6, 6991 (2015).
- [34] M. Gehlmann, I. Aguilera, G. Bihlmayer, S. Nemšák, P. Nagler, P. Gospodarič, G. Zamborlini, M. Eschbach, V. Feyer, F. Kronast, E. Młyńczak, T. Korn, L. Plucinski, C. Schüller, S. Blügel, and C. M. Schneider, Nano Lett. 17, 5187 (2017).
- [35] R. He, J. A. Yan, Z. Yin, Z. Ye, G. Ye, J. Cheng, J. Li, and C. H. Lui, Nano Lett, **16**, 1404 (2016).
- [36] X.-F. Qiao, J.-B. Wu, L.-W. Zhou, J.-S. Qiao, W. Shi, T. Chen, X. Zhang, J. Zhang, W. Ji, and P.-H. Tan, Nanoscale, 8, 8324 (2015).
- [37] See Supplemental Material at http://link.aps.org/supplemental/ 10.1103/PhysRevB.101.174309 for sample characterization, polarization-dependent DT dynamics, and DT measurement of bulk sample.
- [38] Q. Cui, J. He, M. Z. Bellus, M. Mirzokarimov, T. Hofmann, H. Y. Chiu, M. Antonik, D. He, Y. Wang, and H. Zhao, Small 11, 5565 (2015).
- [39] A. Chernikov, A. M. Van Der Zande, H. M. Hill, A. F. Rigosi, A. Velauthapillai, J. Hone, and T. F. Heinz, Phys. Rev. Lett. 115, 126802 (2015).
- [40] E. a. a. Pogna, M. Marsili, D. De Fazio, S. Dal Conte, C. Manzoni, D. Sangalli, D. Yoon, A. Lombardo, A. C. Ferrari, A. Marini, G. Cerullo, and D. Prezzi, ACS Nano 10, 1182 (2016).

- [41] A. Steinhoff, M. Rosner, F. Jahnke, T. O. Wehling, and C. Gies, Nano Lett. 14, 3743 (2014).
- [42] A. Castellanos-Gomez, J. Quereda, H. P. van der Meulen, N. Agrait, and G. Rubio-Bollinger, Nanotechnology 27, 115705 (2016).
- [43] S. Schmitt-Rink and C. Ell, J. Lumin. 30, 585 (1985).
- [44] S. Sim, J. Park, J. G. Song, C. In, Y. S. Lee, H. Kim, and H. Choi, Phys. Rev. B 88, 075434 (2013).
- [45] Y. Z. Ma, L. Valkunas, S. L. Dexheimer, S. M. Bachilo, and G. R. Fleming, Phys. Rev. Lett. 94, 157402 (2005).
- [46] M. Seo, H. Yamaguchi, A. D. Mohite, S. Boubanga-Tombet, J. C. Blancon, S. Najmaei, P. M. Ajayan, J. Lou, A. J. Taylor, and R. P. Prasankumar, Sci. Rep. 6, 21601 (2016).
- [47] H. Wang, C. Zhang, and F. Rana, Nano Lett. 15, 339 (2015).
- [48] H. Wang, C. Zhang, and F. Rana, Nano Lett. 15, 8204 (2015).
- [49] P. Parkinson, H. J. Joyce, Q. Gao, H. H. Tan, X. Zhang, J. Zou, C. Jagadish, L. M. Herz, and M. B. Johnston, Nano Lett. 9, 3349 (2009).
- [50] S. Sim, J. Park, N. Koirala, S. Lee, M. Brahlek, J. Moon, M. Salehi, J. Kim, S. Cha, J. H. Sung, M.-H. Jo, S. Oh, and H. Choi, ACS Photon. 3, 1426 (2016).
- [51] E. Liu, M. Long, J. Zeng, W. Luo, Y. Wang, Y. Pan, W. Zhou, B. Wang, W. Hu, Z. Ni, Y. You, X. Zhang, S. Qin, Y. Shi, K. Watanabe, T. Taniguchi, H. Yuan, H. Y. Hwang, Y. Cui, F. Miao, and D. Xing, Adv. Funct. Mater. 26, 1938 (2016).
- [52] V. Shahnazaryan, I. Iorsh, I. A. Shelykh, and O. Kyriienko, Phys. Rev. B 96, 115409 (2017).
- [53] A. Arora, J. Noky, M. Drüppel, B. Jariwala, T. Deilmann, R. Schneider, R. Schmidt, O. Del Pozo-Zamudio, T. Stiehm, A. Bhattacharya, P. Krüger, S. Michaelis de Vasconcellos, M. Rohlfing, and R. Bratschitsch, Nano Lett. 17, 3202 (2017).
- [54] A. Singh, G. Moody, K. Tran, M. E. Scott, V. Overbeck, G. Berghäuser, J. Schaibley, E. J. Seifert, D. Pleskot, N. M. Gabor, J. Yan, D. G. Mandrus, M. Richter, E. Malic, X. Xu, and X. Li, Phys. Rev. B 93, 041401(R) (2016).
- [55] M. A. Seo, J. Yoo, S. A. Dayeh, S. T. Picraux, A. J. Taylor, and R. P. Prasankumar, Nano Lett. 12, 6334 (2012).
- [56] J. He, D. He, Y. Wang, Q. Cui, F. Ceballos, and H. Zhao, Nanoscale 7, 9526 (2015).
- [57] F. Wang, Y. Wu, M. S. Hybertsen, and T. F. Heinz, Phys. Rev. B 73, 245424 (2006).
- [58] P. Cudazzo, I. V. Tokatly, and A. Rubio, Phys. Rev. B 84, 085406 (2011).
- [59] G. Zhang, S. Huang, F. Wang, Q. Xing, H. Yan, A. Chaves, and T. Low, Sci. Adv. 4, eaap9977 (2018).
- [60] Y. Zhou, H. Tan, Y. Sheng, Y. Fan, W. Xu, and J. H. Warner, ACS Nano 12, 4669 (2018).